Median fin function during the escape response of bluegill sunfish (Lepomis macrochirus). II: Fin-ray curvature

The Journal of Experimental Biology 215, 2881-2890

doi:10.1242/jeb.068593

RESEARCH ARTICLE

Median fin function during the escape response of bluegill sunfish (*Lepomis macrochirus*). II: Fin-ray curvature

Brad A. Chadwell[1], Emily M. Standen[2,*], George V. Lauder[2] and Miriam A. Ashley-Ross[1,†]

[1]Department of Biology, Box 7325, Wake Forest University, Winston-Salem, NC 27109, USA and [2]Museum of Comparative Zoology, Harvard University, 26 Oxford Street, Cambridge, MA 02138, USA

*Present address: Redpath Museum, McGill University, 859 Sherbrooke Street West, Montreal, Quebec, H3A 0C4, Canada
†Author for correspondence (rossma@wfu.edu)

SUMMARY

Although kinematic analysis of individual fin rays provides valuable insight into the contribution of median fins to C-start performance, it paints an incomplete picture of the complex movements and deformation of the flexible fin surface. To expand our analysis of median fin function during the escape response of bluegill sunfish (*Lepomis macrochirus*), patterns of spanwise and chordwise curvature of the soft dorsal and anal fin surfaces were examined from the same video sequences previously used in analysis of fin-ray movement and orientation. We found that both the span and chord undergo undulation, starting in the anterior region of either fin. Initiated early in Stage 1 of the C-start, the undulation travels in a postero-distal direction, reaching the trailing edge of the fins during early Stage 2. Maximum spanwise curvature typically occurred among the more flexible posterior fin rays, though there was no consistent correlation between maximum curvature and fin-ray position. Undulatory patterns suggest different mechanisms of action for the fin regions. In the anterior fin region, where the fin rays are oriented dorsoventrally, undulation is directed primarily chordwise, initiating a transfer of momentum into the water to overcome the inertia of the flow and direct the water posteriorly. Within the posterior region, where the fin rays are oriented caudally, undulation is predominantly directed spanwise; thus, the posterior fin region acts to ultimately accelerate this water towards the tail to increase thrust forces. Treatment of median fins as appendages with uniform properties does not do justice to their complexity and effectiveness as control surfaces.

Supplementary material available online at http://jeb.biologists.org/cgi/content/full/215/16/2881/DC1

Key words: median fin, curvature, C-start, escape response, bluegill.

Received 22 November 2011; Accepted 22 April 2012

INTRODUCTION

Ray-finned fishes (Actinopterygii) derive their name from the bony supports within each membranous paired or median fin. Each fin ray, or lepidotrich, is a segmented bilaminar structure capable of bending and twisting in response to external fluid forces or internal muscular actuation (Alben et al., 2007; Arita, 1971; Geerlink and Videler, 1986; Lauder et al., 2011). Although it is the fin rays that may be actively controlled by the fish, the fin rays by themselves do not define the fin; the membrane connecting the bony supports plays an integral role by providing both surface and tensile resistance that creates the 'fan' of the fin. Individual fin rays may curve, or move laterally or sagittally; such movements of the many fin rays within each fin interact with the flexible membrane, throwing the surface of the 'fan' into complex configurations. Actinopterygian fins are thus flexible structures that interact with the surrounding flow as dynamic curved surfaces (Lauder et al., 2006; Walker, 2004; Walker and Westneat, 2002). Understanding the complex interplay between fin shape and motion during locomotion will provide new insight into the hydrodynamic roles of the fins as control surfaces (Lauder and Drucker, 2004). Therefore, it is essential to quantify fin curvature as well as the motions of individual fin rays (Chadwell et al., 2012) to understand how fins may function.

Although the flexibility of the fins has been well documented (Blake, 1981; Breder, 1926; Lauder, 2006; Osburn, 1906), most recent studies have focused on experimental and computational analysis of fin hydrodynamics, with little emphasis on the individual fin-ray kinematics and curvature (Epps and Techet, 2007; Lauder et al., 2006; Mittal et al., 2006; Tytell and Lauder, 2008). Currently, we know of only two studies that have measured the curvature of individual fin rays during locomotion [dorsal and anal fins of bluegill sunfish (Standen and Lauder, 2005), pectoral fins of longhorn sculpin (Taft et al., 2008)]. However, in both of these studies, curvature was measured only along the length of the fin rays, irrespective of the fin surface. Additionally, the curvature was measured at a single time point of the swimming behavior, providing no information of how the curvature changed over time.

Based on morphological variation among the fin rays of the dorsal and anal fins (Chadwell and Ashley-Ross, 2012), we would expect variation in the potential for curvature as well. Curvature of an individual fin ray is the sum total of bending at the joints between segments of the hemitrichia, and sliding of the individual hemitrichs relative to their long axis (Alben et al., 2007; Geerlink and Videler, 1986; Lauder et al., 2011); therefore, rays with a greater proportion of their total length devoted to segments, and looser connection between the two hemitrichia, should be capable of greater maximum curvature. In both the soft dorsal and anal fins of bluegill, isolated posterior rays demonstrate more segmentation, and looser connection between hemitrichia, than isolated anterior rays (Chadwell and Ashley-Ross, 2012). Therefore, we expect greater capacity for curvature along the length of the rays in the posterior regions of the fins, because of both morphological differences in the rays themselves as well as

less constraint (i.e. lack of connection with stiff spines) on movement of the posterior fin.

Three-dimensional (3-D) kinematic analysis of the rays and spines of the dorsal and anal fins revealed variation in movement and orientation based on position within the fin, suggesting that different regions of the fins were playing distinct roles during the escape response in bluegill (Chadwell et al., 2012). Visual analysis of videos shows that fin surface shape is influenced not just by the changing orientation of the fin rays through time, but also by the curvature within, among and between the fin rays (Fig. 1). This paper examines the spanwise and chordwise curvature of the soft dorsal and anal fin surfaces during the performance of the C-start escape response of bluegill sunfish (*Lepomis macrochirus*). We describe patterns of fin surface curvatures to address two specific questions. First, does fin-ray curvature vary based on position within the fin, as predicted by morphological variation (Chadwell and Ashley-Ross, 2012)? We expect the more flexible posterior rays of the fin to be more susceptible to curvature than the stiffer fin rays of the anterior region. Second, do the kinematic patterns of fin-ray curvature support the hypothesis that the fins are actively resisting opposing hydrodynamic forces during the C-start [as suggested by electromyographic (EMG) data on inclinator muscle activity (Jayne et al., 1996)] and contributing to the thrust forces generated by the fish? If so, we expect the fin surface to exhibit periods where it actively curves into the flow.

We show that the curvature patterns in both soft dorsal and anal fins conform to our expectations based on morphology. Further, the fin surface does behave in a manner consistent with resisting hydrodynamic forces. Complex undulations of the fin surface appear to accelerate water towards the tail, potentially increasing thrust generated during the C-start.

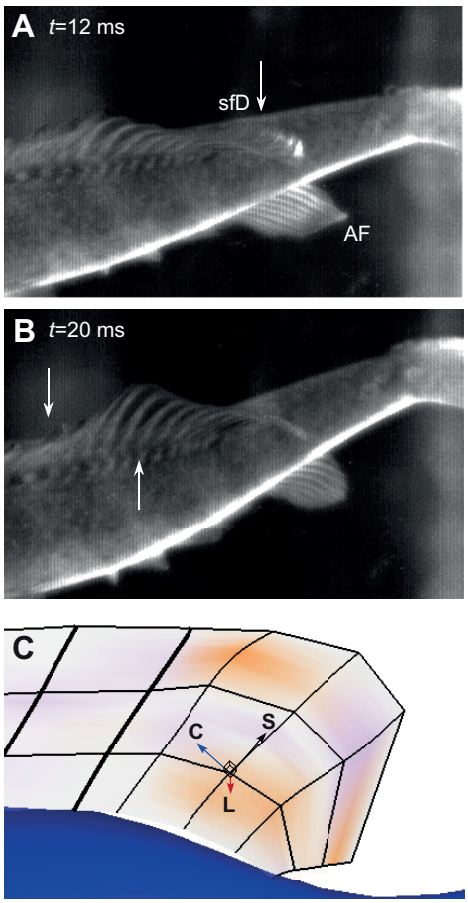

Fig. 1. Curvature in the dorsal fin. Still images from the dorsal view of the C-start of a bluegill sunfish (A) 12 ms and (B) 20 ms after the onset of the escape response. Both the soft dorsal (sfD) and anal fins (AF) can be seen. White arrow in A indicates the formation of an S-curve in the span direction of the fin. The two white arrows in B indicate the chordwise undulation in the fin. (C) Close-up of a reconstructed dorsal fin to show the orientation of the three orthogonal axes of an individual fin ray at a single point: span (**S**), chord (**C**) and lateral (**L**) axes. For details, see the Appendix.

MATERIALS AND METHODS

Animals

Bluegill sunfish, *Lepomis macrochirus* Rafinesque 1819, collected from seined ponds near Concord, MA, USA, were maintained in individual 40 liter aquaria on a 12 h:12 h light:dark photoperiod at a mean water temperature of 20°C (±1°C). The specimens (16–19 cm total length) used in the present study were the same as those examined in the companion paper on 3-D movements and orientation of the dorsal and anal fin spines and rays (Chadwell et al., 2012). In this paper, the term 'fin ray' is used to refer to all external skeletal fin supports when the distinction between spines and rays is disregarded.

Video recording and kinematic analysis

Detailed analysis of fin ray curvatures was performed on the same video sequences as used in the companion paper (Chadwell et al., 2012). Three synchronized high-speed, high-resolution cameras at 500 frames s^{-1} recorded the C-start escape response from a dorsal, ventral and lateral position as the fish maintained a position in the center of the flow tank. Video images from the three cameras were oriented and calibrated for 3-D digitization using a direct linear transformation algorithm (Reinschmidt and van den Bogert, 1997) following a previously described procedure (Standen and Lauder, 2005), and analyzed in the custom digitizing program DigiMat, written by Peter Madden.

Axial kinematics

Axial kinematics were used to determine the metrics of the C-start, e.g. onset of the C-start, timing of Stage 1 (S1) and Stage 2 (S2), turning rates of the body segments associated with the median fins [see fig. 1 in Chadwell et al. (Chadwell et al., 2012)] and the estimated stretched-straight center of mass (ssCOM) movement throughout the duration of the digitized sequences. In two of the nine sequences, the initial C-bend was to the left. To simplify the comparison between the sequences, these sequences were converted to right-handed C-starts by reversing the sign of the *y*-coordinates.

Fin reconstruction

The surfaces of the two median fins at each time point of the escape response were reconstructed as in the companion paper (Chadwell et al., 2012). The four to six points digitized from the selected fin rays [see fig. 1 in Chadwell et al. (Chadwell et al., 2012)] were fit to a cubic smoothing spline with a mean square error of ca. 0.1 mm^3 (Walker, 1998) and 21 equally spaced points along each fin ray were interpolated. The 21 interpolated points from all fin rays of a fin were fit to a bivariate tensor function (Kreyszig, 1991). From this function, we could determine at each point along the lengths of individual fin rays: (1) the orientation of the three axes of the fin ray – span, chord and lateral (Fig. 1C) [also see figs 1, 2 in Chadwell

et al. (Chadwell et al., 2012)] – and (2) the absolute spanwise and chordwise curvature values, where absolute spanwise curvature is the fin surface curvature along the length of the fin ray, i.e. the span axis (synonymous with fin ray curvature reported in Standen and Lauder, 2005; Taft et al., 2008), and absolute chordwise curvature is fin surface curvature perpendicular to the long axis of the fin rays, i.e. the chord axis. It is important to note that because of the changing elevations of the fin rays with longitudinal position in the fins [see figs 1, 2 in Chadwell et al. (Chadwell et al., 2012)], spanwise and chordwise curvature are not aligned with the transverse (or longitudinal) axis of the fish's body. Details of the calculations and nomenclature are found in the Appendix.

Fin-ray curvatures

Previous studies that have examined fin-ray curvature (Standen and Lauder, 2005; Taft et al., 2008) have focused on the absolute spanwise curvature, i.e. bending along the axis of the skeletal supports of the fin. Although absolute spanwise curvature alone provides a measure of the configuration of the fin ray in 3-D space, it fails to provide important information about the direction of the curvature relative to the fin surface for several reasons. First, the values reported do not indicate to which side of the fin surface the curvature is oriented. Second, the spanwise curvature reveals nothing about the interaction among the neighboring rays and the resulting chordwise deformation of the fin surface. Third, these measures invariably include curvature of the rays parallel to, i.e. within, the fin surface, which would introduce confounding results. For example, if the fin were to lie completely flat with the entire surface confined to a single plane, the natural bending of a ray within the plane of the fin (i.e. within the fin membrane itself) would produce spanwise curvature values, though such curvature would not represent functionally meaningful deformation of the fin surface.

To address these issues in our analysis, the absolute spanwise and chordwise curvatures at each point of the fin rays were decomposed into their parallel and perpendicular components relative to the lateral axis, i.e. normal to the fin surface, analogous to decomposing 3-D velocity into its horizontal and vertical components. For the remainder of this paper, spanwise or chordwise curvatures (κ_{span} and κ_{chord}, respectively) will refer only to the components perpendicular to the fin surface. The sign of curvature denotes the direction, relative to the fin surface, with a positive value indicating the concavity faces towards the right of the fin (and the fish) and a negative value indicating left-facing concavity. This technique thus allows us to determine the magnitude and direction of κ_{span} and κ_{chord} along the length of a fin ray, and track changes in those values over time, as the fish performs all the stages of a C-start.

Maximum fin-ray curvatures

For each time point, t, of each fin ray, the maximum positive and negative spanwise and chordwise curvatures were recorded. To facilitate comparison among fin rays throughout the entire escape response, the time and magnitude of three spanwise curvature events were noted for each fin ray: the maximum curvature to the right, $t\kappa_{span0}$ and κ_{span0}, during S1; the maximum curvature to the left, $t\kappa_{span1}$ and κ_{span1}, around the time of S1/S2 transition; and the maximum curvature to the right during S2, $t\kappa_{span2}$ and κ_{span2}. As the maximum spanwise curvature was predicted to be coupled to the turning rate of the mid-trunk, $t\kappa_{span0}$ and $t\kappa_{span1}$ were calculated relative to the time of maximum turning rate of the mid-trunk to the right during S1 ($t\theta'_{max1}$), and $t\kappa_{span2}$ was calculated relative to the time of maximum turning rate of the mid-trunk to the left during S2 ($t\theta'_{max2}$):

$$\Delta t\kappa_{span0} = t\kappa_{span0} - t\theta'_{max1} , \quad (1)$$

$$\Delta t\kappa_{span1} = t\kappa_{span1} - t\theta'_{max1} , \quad (2)$$

$$\Delta t\kappa_{span2} = t\kappa_{span2} - t\theta'_{max2} . \quad (3)$$

Similarly, the time and magnitude of two chordwise curvature events were noted: the maximum curvature to the left, $t\kappa_{chord1}$ and κ_{chord1}, and the maximum curvature to the right, $t\kappa_{chord2}$ and κ_{chord2}. As neither event appeared to be closely associated with maximum turning rate of the body (nor did they consistently occur in either S1 or S2), but rather clustered around rotational transitions, their timings were calculated relative to the time of the change in rotational direction of the body segment ($t\theta'_{tr}$):

$$\Delta t\kappa_{chord1} = t\kappa_{chord1} - t\theta'_{tr} , \quad (4)$$

$$\Delta t\kappa_{chord2} = t\kappa_{chord2} - t\theta'_{tr} . \quad (5)$$

Statistical analysis

As the curvature of the spines of the spiny dorsal fin was negligible, only the fin-ray supports of the soft dorsal and anal fins were analyzed. The anterior-most support of the soft regions of the dorsal and anal fins are the last spines of the fins, DSp10 and ASp3, respectively [see fig. 1 in Chadwell et al. (Chadwell et al., 2012)], and were included in the analyses of the soft dorsal (sfD) and soft anal (sfA) fins. To simplify the incongruity of their numbering, the two spines will be referred to as DSp0 and ASp0. When referring to the fin rays of both dorsal and anal fins collectively, they will be referred to as Sp0, Ry2, Ry5, Ry8 and Ry12. When using a cubic spline, the curvature returned for the end points of a curve is zero; therefore, the final rays of sfD and sfA (DRy12 and ARy12) were excluded from the analysis of chordwise curvature as the chordwise curvature of those fin rays were zero at every position.

Each fin ray is capable of independent movement by its intrinsic musculature; however, the connection between neighboring fin rays by the fin membrane likely contributes to the resulting curvature of the fin ray. Therefore, position effects within sfD and sfA were tested using Friedman's method for randomized blocks (χ^2), using each fish as a block and the fin rays within each group as the treatment levels (Sokal and Rohlf, 1981; Zar, 1984). Bias from pseudo-replication caused by the use of multiple C-start sequences from each fish was avoided by calculating the average values of each kinematic variable, which was ranked between fin rays for each group. Position effect was tested in the average timing and magnitude of the fin ray using the ranked averages from each of the three fish. Additionally, the position effect on the maximal curvature was tested using the ranked maximum curvature achieved by each fin ray (Chadwell et al., 2012). Kendall's coefficient of concordance (W) was calculated to evaluate the degree of concordance between fish (Sokal and Rohlf, 1981; Zar, 1984). Finally, for variables in which a significant position effect was found in both sfD and sfA, a multigroup coefficient of concordance (^cW) was calculated to test whether the position effect was conserved between the two groups (Zar, 1984).

Friedman's χ^2, Kendall's W and their associated P-values were calculated using SPSS v16.0 (IBM, Armonk, NY, USA). A custom program, based on the equations of Zar (Zar, 1984), was written in MATLAB (MathWorks, Natick, MA, USA) to calculate ^cW and its Z-score. To control for Type I errors resulting from multiple comparisons of the 15 variables of each fin group, P-values were

compared with corrected α-levels using a sequential Bonferroni adjustment (Rice, 1989).

RESULTS

Axial movements during the C-start have been described in the companion paper and were shown to be consistent across the three fish analyzed (Chadwell et al., 2012). The curvature parameters of the five fin rays by fish for each fin group can be found in the supplemental material: data for sfD are in supplementary material Table S1 and data for sfA are in supplementary material Table S2.

Spanwise curvature

Within 8–10 ms from the onset of the C-start (T_0) and rotation towards the right by the mid-trunk (Mid), a curvature towards the right, in the direction of the oncoming water flow, began to develop in the proximal region of the posterior fin rays that increased in magnitude as it moved distally along the ray over time (Figs 2, 3).

However, the curving of the fin into the flow of water was short lived; at 12–14 ms from T_0, the proximal regions of the rays began to bend to the left as the mid-trunk rotation to the right slowed down. The curvature also increased in magnitude as it moved distally along the ray over time. During the rotational transition from S1 to S2, a transient S-curve formed along the length of several rays, with ray curvature in the proximal region directed to the left at the same time as the distal region of the ray curved to the right (Figs 2, 3). This S-curve is observable in still images from the video sequence (Fig. 1A) and the digital reconstruction of the fins (supplementary material Movie 1).

A third spanwise curvature of the fin rays, directed to the right, occurred as the turning rate of the mid-trunk to the left increased during S2 (18–50 ms after T_0), as Mid rotated to the left. This curvature towards the right appeared first in the proximal region of the fin rays and traveled distally along the ray lengths, but magnitude of maximum curvature was approximately equal along the fin-ray lengths (Figs 2, 3).

The degree of curvature and variation between fin rays and along the ray lengths appeared greater during S1 and the S1/S2 transition than during S2 (Figs 2–4). For both sfD and sfA, all three maximum κ_{span} values increased among the posterior fin rays (Fig. 4). In both fins, a significant position effect was found for mean and maximal κ_{span0} but not for κ_{span1}; for mean κ_{span2}, a significant position effect was found only for sfA (sfD mean and max. κ_{span0}: both W=0.91, χ^2=10.93, P=0.003; mean κ_{span1}: W=0.80, χ^2=9.60, P=0.017; max. κ_{span1}: W=0.82, χ^2=9.87, P=0.015; Table 1; sfA mean κ_{span0}: W=0.96, χ^2=11.47, P=0.001; max. κ_{span0}: W=1.00, χ^2=12.00, P=0.000; mean and max. κ_{span1}: W=0.82, χ^2=9.87, P=0.015; Table 2). $\Delta t\kappa_{span0}$ was nearly synchronous with the time of maximum turning rate of the Mid-trunk, with $\Delta t\kappa_{span1}$ occurring shortly afterward (Fig. 4A,C). $\Delta t\kappa_{span2}$ occurred shortly before Mid reached its maximum turning rate to the left (Fig. 4E). Position effects were not found in any time parameter (sfD $\Delta t\kappa_{span0}$: W=0.56, χ^2=6.67, P=0.163; $\Delta t\kappa_{span1}$: W=0.82, χ^2=9.87, P=0.015; $\Delta t\kappa_{span2}$: W=0.47, χ^2=5.60, P=0.253; Table 1; sfA $\Delta t\kappa_{span0}$: W=0.49, χ^2=5.87, P=0.236; $\Delta t\kappa_{span1}$: W=0.56, χ^2=6.67, P=0.163; $\Delta t\kappa_{span2}$: W=0.31, χ^2=3.73, P=0.493; Table 2).

Over the course of the C-start, the greatest spanwise curvatures, in either direction, typically occurred during the rotational transition of the mid-trunk (14–26 ms), as the turning rate to the right decreased and changed direction to the left (Figs 2, 4). It is also during this time that many of the rays developed an S-curve as the proximal and distal regions curved in opposite directions (Fig. 1A, Figs 2, 3).

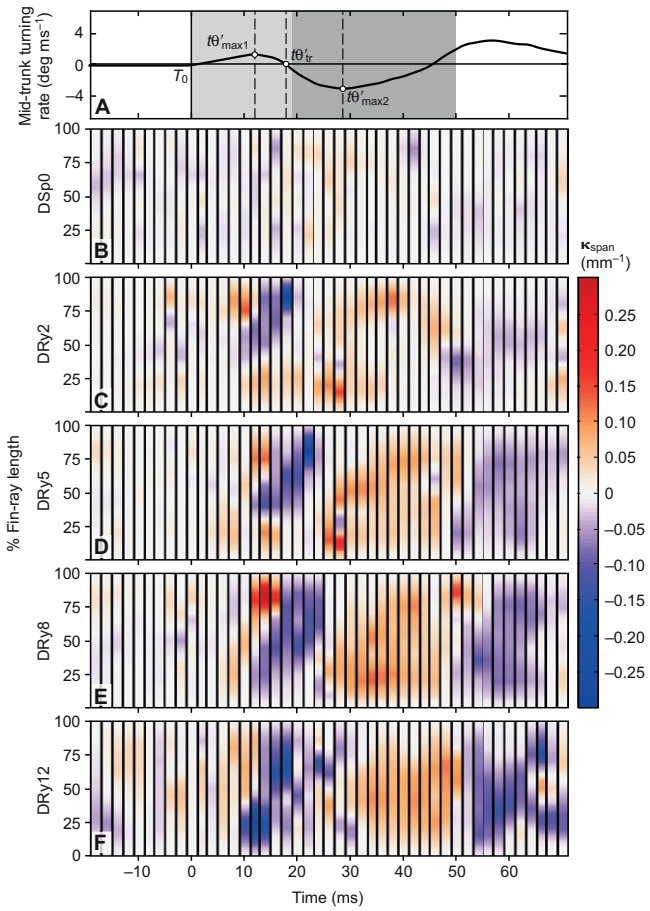

Fig. 2. Spanwise curvature of the soft dorsal fin rays over time. (A) Turning rate of Mid and its three kinematic events, maximum Stage 1 turning rate ($t\theta'_{max1}$), rotational transition ($t\theta_{tr}$) and maximum Stage 2 turning rate ($t\theta'_{max2}$), indicated by the white dots, shown to provide reference for the curvature of the associated fin rays. The light gray region indicates the period of Stage 1, starting from T_0 (onset of C-start), and the darker grey region indicates the period of Stage 2. (B–F) Spanwise curvature along the percent length of each fin ray within the soft dorsal fin group (sfD) for each time point of a single C-start sequence. Color bar represents the intensity and direction of the spanwise curvature, with positive values (orange–red–dark red) indicating spanwise curvature to the right and negative values (purple–blue–dark blue) indicating spanwise curvature to the left. Data in all panels of this figure and Figs 3, 5, 6 and 8 are from the same representative sequence.

Chordwise curvature

Unlike spanwise curvature, chordwise curvature along the length of the fin rays was generally uniform, with only an occasional change in direction (Figs 5, 6, supplementary material Movie 2). Instead, changes in the direction of chordwise curvature typically occurred between rays, particularly between Sp0 and Ry2. Alternating changes in chordwise curvature between fin rays indicates an S-curve in the chord length of the fins (Figs 5, 6), which can be seen in the still images from the video sequence (Fig. 1B) and the digital reconstruction (supplementary material Movie 2).

During S1 rotation of the Mid-trunk to the right, chordwise curvature of the anterior fin surface was directed towards the left. The time of maximum chordwise curvature towards the left ($\Delta t\kappa_{chord1}$) was nearly synchronous with the rotational transition of the mid-trunk, $t\theta'_{tr}$, with the greatest curvature occurring at Ry2 (Fig. 7A,B). A significant position effect was found only for maximal κ_{chord1} of sfA

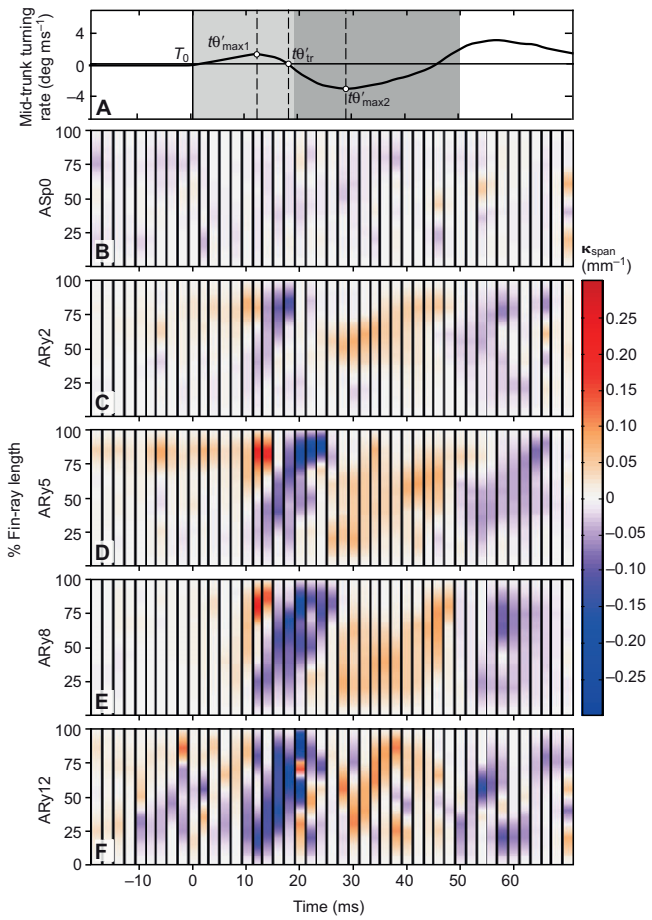

Fig. 3. Spanwise curvature of the anal fin rays over time. (A) Turning rate of Mid and its three kinematic events, shown to provide reference for the curvature of the associated fin rays. (B–F). Spanwise curvature along the percent length of each fin ray within the anal fin group (sfA) for each time point of a single C-start sequence. Symbols, shading and color bar as in Fig. 2.

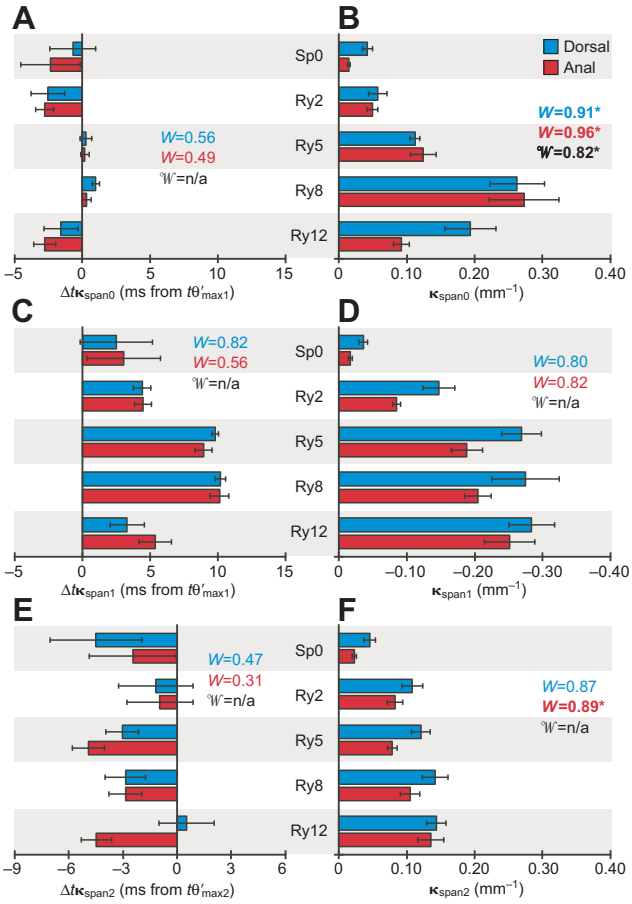

Fig. 4. Spanwise curvature parameters of the fin rays. (A) Average timing of the initial maximum spanwise curvature to the right. (B) Average of the initial maximum spanwise curvature to the right. (C) Average timing of the following maximum spanwise curvature to the left. (D) Average of the following maximum spanwise curvature to the left. (E) Average timing of the second maximum spanwise curvature to the right. (F) Average of the second maximum spanwise curvature to the right. All timing parameters are in relation to the corresponding time event of the Mid-trunk turning rate, $t\theta'_{event}$. For each parameter, Kendall's coefficient of concordance, W, and, if applicable, the multigroup coefficient of concordance, $\mathcal{W}$, are provided. Significant position effects are indicated in bold with an asterisk. Bars are means ±1 s.e.m., N=9 sequences from three fish.

(W=0.98, χ^2=8.79, P=0.004; all other variables were non-significant after Bonferroni correction; Tables 1, 2).

As the mid-trunk rotated to the left during S2, the chord surface was curved to the right (Fig. 7C,D). The time of maximum chordwise curvature to the right ($\Delta t\kappa_{chord2}$) followed $t\theta'_{tr}$, as the Mid-trunk began its rotation to the left, with κ_{chord2} more uniform among the fin rays (Fig. 7C,D). No significant position effects were found for either sfD or sfA (Tables 1, 2).

As with the spanwise curvature, the location of maximum chordwise curvature changed over time, moving posteriorly along the chord of the fin, indicating a traveling wave of chordwise curvature.

Dorsal *versus* anal fins

Of the 15 curvature parameters, significant position effects in both sfA and sfD were found only for mean and maximal κ_{span0} (Tables 1, 2), both of which showed a significant degree of concordance between sfD and sfA ($\mathcal{W}\geq0.8$, $Z\geq4.8$, $P<0.0001$).

DISCUSSION

The dorsal and anal fins of bluegill are integral to the performance of the C-start, moving in patterns that suggest an active role in interacting with the surrounding fluid. Regions of the median fins differ in their mobility and flexibility, which we suggest affects their function in the escape response. Understanding how the median fins contribute to the C-start necessitates combining data regarding movements of the axial body and individual fin rays with measures of fin curvature. Detailed fin kinematics may be subsequently correlated with EMG and hydrodynamic data to suggest the function of median fins during the escape response.

Median fin kinematics during the C-start: a synthesis

The escape response is traditionally broken down into two consistent stages (S1 and S2) and one variable stage (S3), plus transitions between those stages, based on movements of the rostrum (Domenici and Blake, 1997; Wakeling, 2001). Changes in fin configuration follow the major kinematic events described for the body, with consistent patterns for S1, the S1/S2 transition and S2.

At T_0, the dorsal and anal fins are typically partially splayed and in line with the sagittal midline of the body. Curvature values are

Table 1. Kendall's *W* and Friedman's χ^2 for soft dorsal fin-ray curvature parameters

	ΔTime			Mean κ			Max. κ		
Parameter	*W*	χ^2	*P*	*W*	χ^2	*P*	*W*	χ^2	*P*
Spanwise curvature									
span0	0.56	6.67	0.163	**0.91**	**10.93**	**0.003**	**0.91**	**10.93**	**0.003**
span1	0.82	9.87	0.015	0.80	9.60	0.017	0.82	9.87	0.015
span2	0.47	5.60	0.253	0.87	10.40	0.005	0.75	9.02	0.029
Chordwise curvature									
chord1	0.84	7.55	0.028	0.70	6.31	0.108	0.87	7.82	0.0208
chord2	0.64	5.80	0.148	0.64	5.80	0.148	0.54	4.86	0.208

ΔTime is the difference in time of a given parameter (individual rows) from the corresponding kinematic event of the Mid-trunk ($t\theta'_{event}$). Mean κ is the average curvature for all sequences for each fish. Max. κ is the maximal curvature that was achieved by the fish, observed in any sequence. See text for details. Significant analyses with *P*-values less than their adjusted α-levels are indicated in bold. For κ_{span}, d.f.=2, 4; for κ_{chord}, d.f.=2, 3.

uniformly low in both span and chord axes (Figs 2, 3, 5, 6). Little movement of the fins occurs until approximately one-third of the way through S1, when the soft fin rays begin a sweep to the left [see fig. 9 in Chadwell et al. (Chadwell et al., 2012)], as if they were being moved passively by the resistance of the water. However, there is reason to suspect that the fin rays are not simply passive structures; spanwise curvature of the rays is to the right, into the flow, as if the fin ray musculature were contracting and causing the ray to bend through differential sliding of the hemitrichia (Alben et al., 2007; Lauder et al., 2011). These observations match the EMG patterns of the dorsal inclinators of bluegill sunfish during a C-start (Jayne et al., 1996), which have been shown to induce fin-ray curvature to the same side of activity (Arita, 1971; Geerlink and Videler, 1986). At the onset of the C-start, a brief period of activity in the dorsal inclinator muscles, ipsilateral to the initial C-bend, was synchronous with activity in the axial musculature. The initial spanwise curvature of the fin rays to the right coincides with this activity, and supports the hypothesis that the fins are actively resisting opposing forces. The little chordwise curvature that occurs, cupping the fin towards the right into the flow, may simply be the result of axial curvature of the body, rather than movement of the fins *per se*.

In the latter half of S1, as the Mid-trunk is slowing down (i.e. after $t\theta'_{max1}$; Figs 2, 3, 5, 6), the rays of the soft fins sweep in the opposite direction, i.e. towards the right [see fig. 9 in Chadwell et al. (Chadwell et al., 2012)]. At the same time, magnitudes of both spanwise and chordwise curvature increased, but in complex ways. In general, the posterior regions of the soft fins (e.g. rays 8–12) are the least constrained by the connection both between hemitrichia and with neighboring rays, and thus tend to show more multidirectional curvature patterns. For example, examination of Figs 2, 3 and Fig. 8C,D reveals that individual rays are thrown into S-curves [DRy8 and ARy12 are the most extreme examples; at 12–20 ms, they are curved strongly towards one side in the proximal portions, with (sometimes multiple) curves towards the other side in the distal regions]. Likewise, Fig. 5 shows that at the same time points, chordwise curvature undulates along the length of the fin as a whole (left curvature at DSp0, right at DRy2, left at DRy5, and then right again at DRy8), with the greatest magnitude at the distal ends of the rays. In both spanwise and chordwise directions, curvature of the fin surface propagates along the length of the rays (curvature along the axis of the individual rays; diagonal progression of color regions within panels in Figs 2, 3) and the chord of the fin (curvature normal to the span axis of the individual rays; diagonal progression of color regions between panels in Figs 5, 6), setting up the global undulation of the fin that will shed vortices during S2.

At the time of the rotational transition of the Mid-trunk, the fin rays continue sweeping to the right [see fig. 9 in Chadwell et al. (Chadwell et al., 2012)], while spanwise curvature is directed to the left of the fish (Figs 2, 3, Fig. 8E). As the Mid-trunk is now moving to the left, once again the spanwise curvature of the rays is directed into the flow. It is interesting to note that Jayne et al. reported that onset of EMG activity among the contralateral dorsal inclinators occurred prior to the end of trunk rotation to the right (Jayne et al., 1996), suggesting some active role in fin-ray position and curvature. However, it is unclear whether contraction of the fin musculature is sufficient to stiffen and curve the rays against the flow, or if the curvature direction is maintained at this time simply because the resistance of the water has not 'caught up' with the fin surface.

In the initial part of S2, the fin rays continue their sweep to the right, reaching maximum sweep angle prior to the time of maximum turning rate of Mid to the left [see fig. 9 in Chadwell et al. (Chadwell et al., 2012)]. At the same time, the wave of left-directed spanwise curvature is being shed from the distal ends of the rays, particularly in the posterior region of the fins (Figs 2,

Table 2. Kendall's *W* and Friedman's χ^2 for anal fin-ray curvature parameters

	ΔTime			Mean κ			Max. κ		
Parameter	*W*	χ^2	*P*	*W*	χ^2	*P*	*W*	χ^2	*P*
Spanwise curvature									
span0	0.49	5.87	0.236	**0.96**	**11.47**	**0.001**	**1.00**	**12.00**	**0.000**
span1	0.56	6.67	0.163	0.82	9.87	0.015	0.82	9.87	0.015
span2	0.31	3.73	0.493	**0.89**	**10.67**	**0.004**	0.82	9.87	0.015
Chordwise curvature									
chord1	0.20	1.80	0.727	0.47	4.20	0.300	**0.98**	**8.79**	**0.004**
chord2	0.56	5.00	0.207	0.29	2.59	0.545	0.31	2.79	0.500

See Table 1 for the description of ΔTime, Mean κ and Max. κ. See text for a description of the parameters. Significant analyses with *P*-values less than their adjusted α-levels are indicated in bold. For κ_{span}, d.f.=2, 4; for κ_{chord}, d.f.=2, 3.

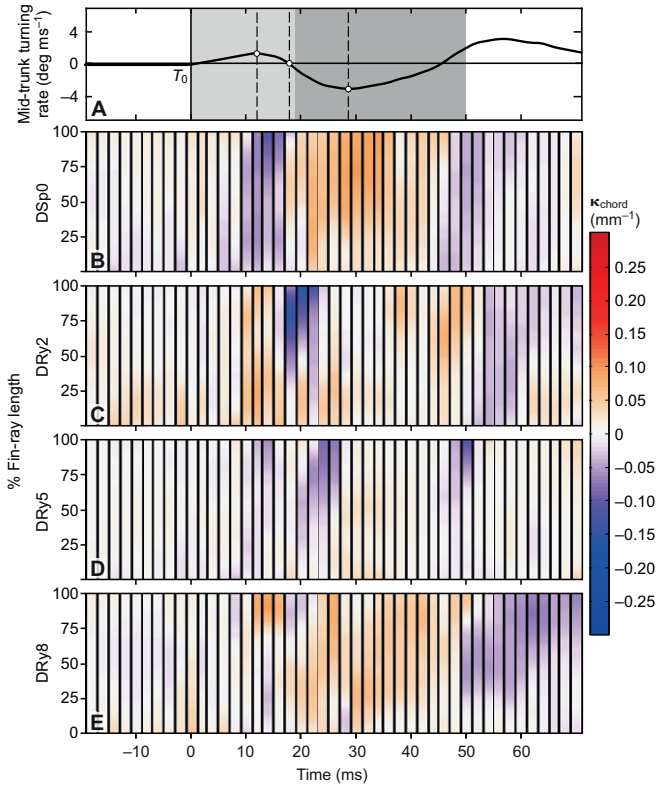

Fig. 5. Chordwise curvature of the soft dorsal fin rays over time. (A) Turning rate of Mid and its three kinematic events, shown to provide reference for the curvature of the associated fin rays. (B–E) Chordwise curvature (perpendicular to the span axis) along the percent length of each fin ray within the soft dorsal fin group (sfD) for each time point of a single C-start sequence. Color bar represents the intensity and direction of chordwise curvature, with positive values (orange–red–dark red) indicating chordwise curvature to the right and negative values (purple–blue–dark blue) indicating chordwise curvature to the left. Symbols and shading as in Fig. 2.

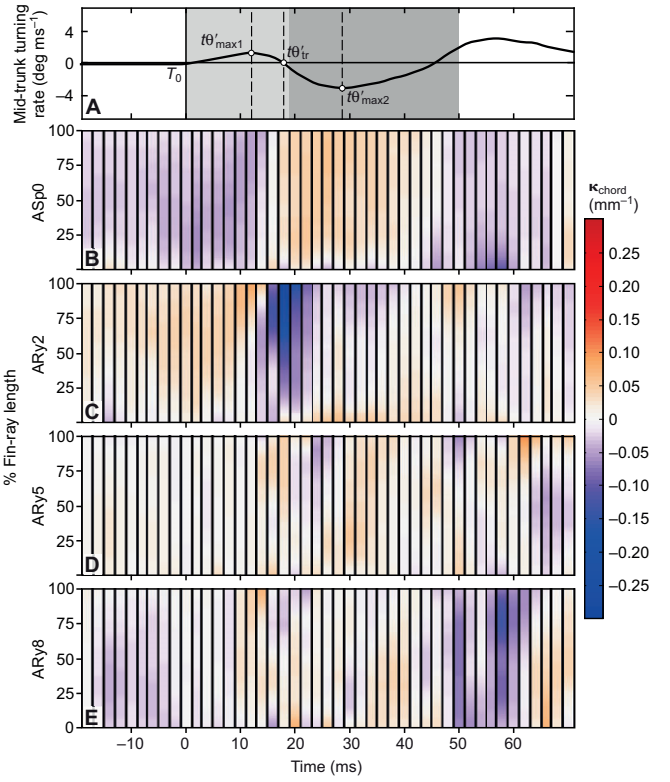

Fig. 6. Chordwise curvature of the anal fin rays over time. (A) Turning rate of Mid and its three kinematic events; shown to provide reference for the curvature of the associated fin rays. (B–E) Chordwise curvature (perpendicular to the span axis) along the percent length of each fin ray within the anal fin group (sfA) for each time point of a single C-start sequence. Symbols and shading as in Fig. 2. Color bar as in Fig. 5.

3, Fig. 8F,G). A new spanwise curvature of the fin to the right, directed away from the flow, in the proximal portions of the rays develops soon after the rotational transition of the mid-trunk (Fig. 8G). The muscular activity of the dorsal inclinators found during S2 (Jayne et al., 1996) may be actively resisting the opposing hydrodynamic forces, but does not appear to be able to completely prevent fin-ray bending. Chordwise undulation of the fins in the anterior regions (Sp0, Ry2 and Ry5) propagates posteriorly and, because of the changing angle of the fin rays relative to the body axis (Fig. 8), is transformed to spanwise undulation of the fin rays in the posterior region (Ry8, Ry12; discussed further in Hydrodynamic implications, below).

During the final portion of S2, when the Mid-trunk is slowing (after $t\theta'_{max2}$), the motions and curvature of the fin rays mirror those seen towards the end of S1. The rays begin to sweep towards the left, into the flow and towards the midline of the body [see fig. 9 in Chadwell et al. (Chadwell et al., 2012)], and both spanwise and chordwise curvature are directed towards the right, away from the flow, as if the tips of the fin rays lag behind the bases (Figs 2, 3, 5, 6). Jayne et al. reported activity in the contralateral dorsal inclinator muscles throughout S2 (Jayne et al., 1996); it is possible that the sweep of the rays to the left is driven by this contraction, which may be able to overcome hydrodynamic forces only as the trunk slows down.

Movements and curvature of the dorsal and anal fins during the S2/S3 transition and S3 are highly variable, reflecting the multitude of behaviors demonstrated by fish, e.g. braking, gliding to a stop, initiating a second propulsive stroke, etc. As a result, no consistent pattern in fin configuration exists for this portion of the C-start.

Comparisons with other studies of fin curvature

Previous studies that have examined the function of the dorsal and anal fins have demonstrated that their movement and conformation vary with the locomotor behavior (e.g. steady swimming, maneuvering, braking, etc.), with deformation being greatest in the posterior regions of the fins, i.e. the trailing edge (Drucker and Lauder, 2001b; Drucker and Lauder, 2005; Jayne et al., 1996; Lauder and Drucker, 2004; Standen and Lauder, 2005). Of these studies, most observations have comprised strictly qualitative remarks on fin shape; only one measured the absolute spanwise curvature of individual fin rays. Standen and Lauder examined dorsal and anal fin movement in bluegill during steady swimming at various speeds and during slow yaw maneuvers, measuring curvature at the point of maximum excursion by the fins (Standen and Lauder, 2005). Although they found that the average maximum curvature differed between fin rays within a single fin, no consistent pattern was observed in those differences among speeds or individuals. Rather, a significant difference in curvature was found when comparing different behaviors, with overall fin-ray curvature greater during slow turning maneuvers than in steady swimming at low speeds [$\leq$1.0 TL s^{-1} (Standen and Lauder, 2005)]. Similarly, our results show

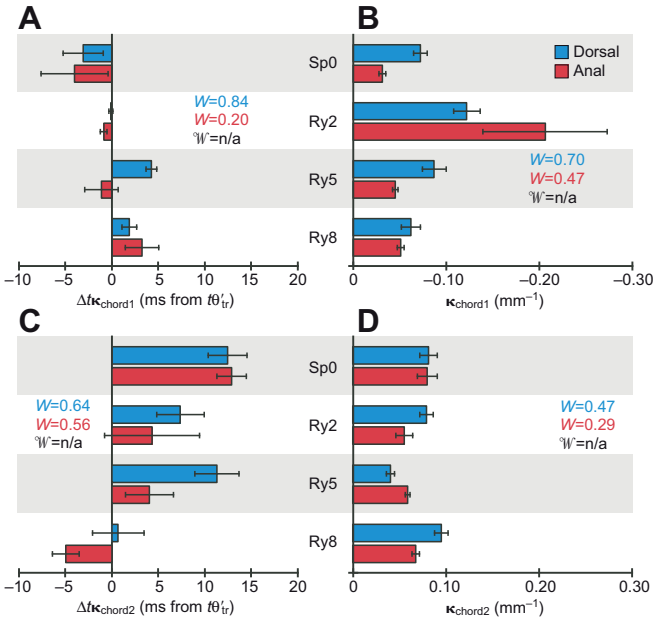

Fig. 7. Chordwise curvature parameters of the fin rays. (A) Average timing of the maximum chordwise curvature to the left. (B) Average of the maximum chordwise curvature to the left. (C) Average timing of the maximum chordwise curvature to the right. (D) Average of the maximum chordwise curvature to the right. Symbols as in Fig. 4.

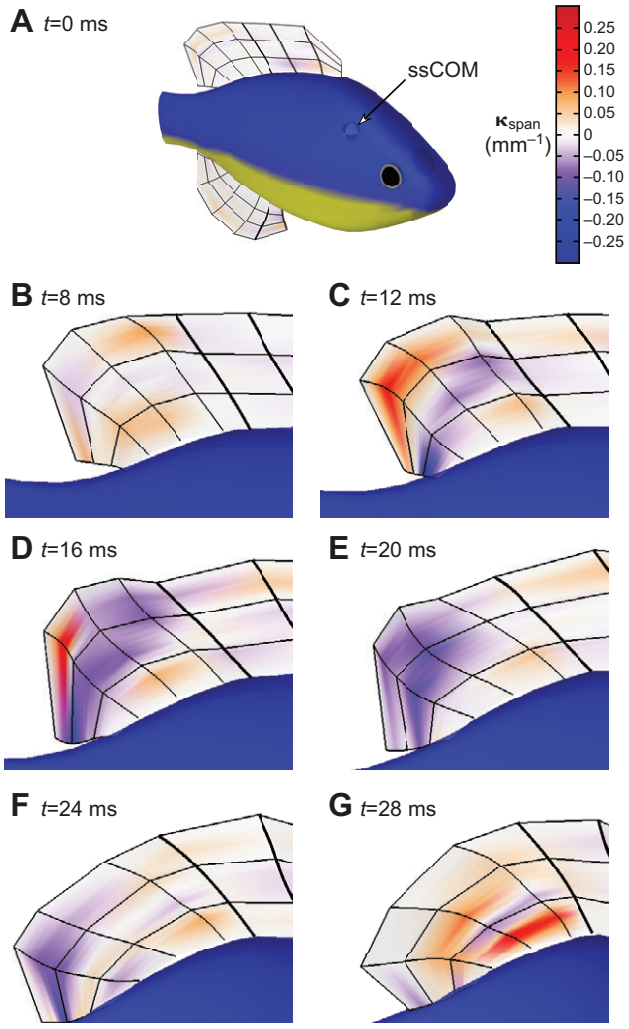

Fig. 8. Reconstructed bluegill median fins. The digitally reconstructed bluegill displaying the spanwise curvature across the median fins at different time points over the C-start. (A) Representation of the fish axis, estimated stretched-straight center of mass (ssCOM) and median fins prior to the onset of the C-start (t=0 ms). (B–G) Close-up images of the soft dorsal fin at consecutive time points. Color bar as in Fig. 2

that patterns of maximum spanwise and chordwise curvature of the fin rays were statistically inconsistent (Figs 4, 7), though the posterior rays typically showed the greatest degree of spanwise curvature. Curvature magnitudes are strikingly different between the present study (mean maximum curvature ca. 0.28 mm^{-1}) and that of Standen and Lauder, where they reported mean maximum values of ca. 0.08 mm^{-1} (Standen and Lauder, 2005). The nearly threefold increase in mean curvature magnitude between slow maneuvering and the fast-start escape response highlights the scope for deformation of fin rays in response to behavioral demands.

Studies of pectoral fin kinematics have also demonstrated the flexible nature of actinopterygian fins (Lauder et al., 2006; Lauder and Madden, 2007; Ramamurti et al., 2002; Taft et al., 2008). Curvature into the flow has been observed in the pectoral fin of the bluegill during turning maneuvers (Drucker and Lauder, 2001a), supporting the hypothesis that fin rays are under active control by their intrinsic musculature, as we have postulated for the median fins. Despite a number of hydrodynamic studies, to our knowledge only one paper has reported individual spanwise fin-ray curvature and shown that the degree of curvature differs not only between behaviors (steady swimming *versus* station holding) but among the individual rays (Taft et al., 2008). Despite the obvious differences in the shape and use of pectoral and median fins, both types of fins share a similar structure and act as control surfaces to modulate hydrodynamic forces.

Standen and Lauder suggested that the overall conformation, or fin shape, is achieved to some extent by the summation of spanwise curvature but also differences in the movements of individual fin rays (Standen and Lauder, 2005). The present results and those of the companion paper (Chadwell et al., 2012) support the hypothesis that differences in orientation of the fin rays, resulting from rotation at the fin-ray joint (sweep, span axis rotation and elevation), produce chordwise curvature of the fin; this combines with spanwise curvature of the fin rays to determine overall fin shape. Our studies have tracked both the timing and magnitude of both spanwise and chordwise curvatures throughout the entire C-start sequence to show the dynamic nature of fin shape over time (supplementary material Movies 1, 2). With such understanding, we can begin to connect how movement and conformation of the fin surfaces contributes to the hydrodynamic forces generated during the behavior.

Hydrodynamic implications

During the C-start, both the soft dorsal and anal fins demonstrate undulatory waves that spread across their surfaces in a postero-distal direction (Fig. 8, supplementary material Movies 1, 2). The movement of the median fins coincides with the generation of a fluid jet ('jet two') by the body and fins that results in production of thrust forces that propel the fish away from the threat during the escape response (Borazjani et al., 2012; Tytell and Lauder, 2008).

Regional variation in curvature kinematics suggests functionally distinct roles in generating momentum. We propose

that the initial chordwise curvature in the anterior region of the fins assists the body in initiating the movement of fluid, overcoming the inertia of the water during S1. In S2, as the fish is accelerating away from the threat, the volume of water must be moved posteriorly, towards the tail, if the fish is to gain thrust from the jet. Lateral undulation of the body moves the bulk of jet two towards the tail; the dorsal and anal fins contribute their own portions of jet two (Tytell and Lauder, 2008), and are responsible for moving the associated water. Therefore, the chordwise traveling wave of undulation begins the requisite movement. However, in the posterior region of both soft fins, the rays are directed more caudally than dorsally or ventrally. In these posterior regions, chordwise undulation would not act to continue moving the fluid towards the tail. Instead, spanwise undulation along the lengths of posterior rays allows the fluid to continue in its trajectory so that it may be finally shed from the trailing edge of the median fins and interact with the caudal fin, generating ca. 37% of the total momentum associated with the C-start (Tytell and Lauder, 2008).

Together, the present paper and its companion (Chadwell et al., 2012) comprise studies that are the first to reconstruct the orientation, movements and curvatures of individual fin rays, and the complete fin surface throughout the duration of the C-start escape response. The patterns observed provide evidence to support the hypothesis that fin rays are resisting opposing hydrodynamic forces by muscular activity and/or the intrinsic biomechanical properties derived from their morphology. Future comparative studies are needed to determine the active muscular control over the different regions of the median fins during the escape response, as are examinations of function of median fins that possess different underlying structure, shape or skeletal modifications (e.g. adipose dorsal fins of trout, sickle-shaped median fins in scombrids, unsegmented ceratotrich-supported median fins in elasmobranchs). By combining detailed kinematic analysis of the fin surface with morphological, EMG and hydrodynamics studies, we gain greater insight into the complex ways in which fish control a vitally important behavior.

APPENDIX

To construct each fin surface, the eight dorsal (and six anal) fin rays, r, and their 21 interpolated points, p (as described in the Materials and methods), were each fit to a bivariate, cubic tensor spline function:

$$f(r,p). \tag{A1}$$

By holding one variable constant, the bivariate tensor function can be differentiated with respect to the other variable to generate the partial derivatives, which can be used to calculate the spanwise and chordwise parameters of the fin surface at any given position, $P_{(a,b)}$, where the subscript 'a' represents a given fin ray and the subscript 'b' represents a given point along the fin ray's length. The first and second partial derivatives with respect to p as r is held constant (f_p and f_{pp}, respectively) describe the spanwise curve of the fin surface along the points of each individual fin ray:

$$f_p = \frac{\partial f}{\partial p}, \tag{A2}$$

$$f_{pp} = \frac{\partial^2 f}{\partial p^2}. \tag{A3}$$

From these partial derivatives, the spanwise tangent (**sT**) and binormal (**sB**) vectors of the fin surface at $P_{(a,b)}$ can be determined:

$$\mathbf{sT}_{(a,b)} = f_{p(a,b)}, \tag{A4}$$

$$\mathbf{sB}_{(a,b)} = f_{p(a,b)} \times f_{pp(a,b)}. \tag{A5}$$

To describe the chordwise curve of the fin surface across each fin ray at the same point along their lengths, the first and second partial derivatives with respect to r as p is held constant (f_r and f_{rr}, respectively) can be calculated:

$$f_r = \frac{\partial f}{\partial r}, \tag{A6}$$

$$f_{rr} = \frac{\partial^2 f}{\partial r^2}. \tag{A7}$$

From which the chordwise tangent (**cT**) and binormal (**cB**) vectors of the fin surface at $P_{(a,b)}$ can be determined:

$$\mathbf{cT}_{(a,b)} = f_{r(a,b)}, \tag{A8}$$

$$\mathbf{cB}_{(a,b)} = f_{r(a,b)} \times f_{rr(a,b)}. \tag{A9}$$

Using the spanwise and chordwise tangents, the three orthogonal axes of each fin ray, at $P_{(a,b)}$, can be calculated: the span axis, **S**, which is parallel to the fin surface and **sT**, i.e. the long axis of the fin ray; the lateral axis, **L**, which is perpendicular to the fin surface and **S** at $P_{(a,b)}$; and the chord axis, **C**, which is parallel to the fin surface but perpendicular to **S** and **L**:

$$\mathbf{S}_{(a,b)} = \frac{\mathbf{sT}_{(a,b)}}{\left|\mathbf{sT}_{(a,b)}\right|}, \tag{A10}$$

$$\mathbf{L}_{(a,b)} = \frac{\mathbf{cT}_{(a,b)} \times \mathbf{sT}_{(a,b)}}{\left|\mathbf{cT}_{(a,b)} \times \mathbf{sT}_{(a,b)}\right|}, \tag{A11}$$

$$\mathbf{C}_{(a,b)} = \frac{\mathbf{L}_{(a,b)} \times \mathbf{S}_{(a,b)}}{\left|\mathbf{L}_{(a,b)} \times \mathbf{S}_{(a,b)}\right|}. \tag{A12}$$

For either fin (dorsal or anal), $\mathbf{S}_{(a,b)}$ is directed towards the distal end of the fin ray, $\mathbf{L}_{(a,b)}$ is directed towards the left side of the fin surface and $\mathbf{C}_{(a,b)}$ is directed towards the anterior edge of the fin ray (Fig. 4B,C). With the **S**-, **L**- and **C**-axes, the orientation of the fin rays, relative to the planes of the body segment to which the fin rays attach (i.e. anterior trunk for the spiny dorsal fin, and Mid-trunk for the soft dorsal and anal fins), were calculated [see fig. 2 in Chadwell et al. (Chadwell et al., 2012)]. At $P_{(a,b)}$, sweep (ω, rotation about the chord axis) was calculated as the angle between $\mathbf{S}_{(a,b)}$ and the sagittal plane of the body segment. Span axis rotation (α) was calculated as the angle between $\mathbf{C}_{(a,b)}$ and the sagittal plane of the body segment. Elevation (ϕ, rotation about the lateral axis) was calculated as the angle between $\mathbf{S}_{(a,b)}$ and the frontal plane of the body segment.

The absolute spanwise curvatures ($|\boldsymbol{\kappa}_{span}|$) of the fin ray at $P_{(a,b)}$ were calculated using **sT** and **sB** (Eqns A4 and A5) as follows:

$$\left|\boldsymbol{\kappa}_{span(a,b)}\right| = \frac{\left|\mathbf{sB}_{(a,b)}\right|}{\left|\mathbf{sT}_{(a,b)}\right|^3}. \tag{A13}$$

The absolute chordwise curvatures ($|\boldsymbol{\kappa}_{chord}|$) of the fin ray at $P_{(a,b)}$ were calculated using **cT** and **cB** (Eqns A8 and A9) as follows:

$$\left|\boldsymbol{\kappa}_{chord(a,b)}\right| = \frac{\left|\mathbf{cB}_{(a,b)}\right|}{\left|\mathbf{cT}_{(a,b)}\right|^3}. \tag{A14}$$

LIST OF SYMBOLS AND ABBREVIATIONS

ARy#	anal ray, where # indicates its numbered position within the fin
ASp#	anal spine, where # indicates its numbered position within the fin
C	chord axis of the fin surface, perpendicular to the span axis
cT	tangent to the chordwise curve
DRy#	dorsal ray, where # indicates its numbered position within the fin
DSp#	dorsal spine, where # indicates its numbered position within the fin
EMG	electromyography
L	lateral axis, normal to the fin surface
Mid	middle trunk
r	fin-ray identifier
S	span axis of the fin surface
S1	stage 1 of the C-start
S2	stage 2 of the C-start
sB	binormal to the fin surface
sfA	soft region of the anal fin
sfD	soft dorsal fin
ssCOM	stretched-straight center of mass
sT	tangent to the spanwise curve
t	time point during a C-start sequence
T_0	time zero
tr	directional transition event, i.e. change in direction of rotation or orientation
tX	time of a given parameter, where X is the event of a given parameter
ΔtX	time difference between a given fin-ray parameter and its corresponding axial event, where X is the event of a given parameter
κ_{chord}	chordwise curvature, perpendicular to the fin surface and span axis
κ_{span}	spanwise curvature, perpendicular to the fin surface
θ'	turning rate, i.e. the first time derivative of yaw

ACKNOWLEDGEMENTS

We thank Peter Madden for writing DigiMat, the custom video analysis program used in this study. We also thank two anonymous reviewers for constructive comments that improved the manuscript.

FUNDING

This work was supported by the National Science Foundation [grant IBN-0316331 to M.A.A.-R. and grant EFRI-0938043 to G.V.L.] and a Vecellio Fund Fellowship to B.A.C.

REFERENCES

Alben, S., Madden, P. G. and Lauder, G. V. (2007). The mechanics of active fin-shape control in ray-finned fishes. *J. R. Soc. Interface* **4**, 243-256.

Arita, G. S. (1971). A re-examination of the functional morphology of the soft-rays in teleosts. *Copeia* **1971**, 691-697.

Blake, R. W. (1981). Influence of pectoral fin shape on thrust and drag in labriform locomotion. *J. Zool.* **194**, 53-66.

Borazjani, I., Sotiropoulos, F., Tytell, E. D. and Lauder, G. V. (2012). Hydrodynamics of the bluegill sunfish C-start escape response: three-dimensional simulations and comparison with experimental data. *J. Exp. Biol.* **215**, 671-684.

Breder, C. M. (1926). The locomotion of fishes. *Zoologica* **6**, 159-297.

Chadwell, B. A. and Ashley-Ross, M. A. (2012). Musculoskeletal morphology and regionalization within the dorsal and anal fins of bluegill sunfish (*Lepomis macrochirus*). *J. Morphol.* **273**, 405-422.

Chadwell, B. A., Standen, E. M., Lauder, G. V. and Ashley-Ross, M. A. (2012). Median fin function during the escape response of bluegill sunfish (*Lepomis macrochirus*). I: Fin-ray orientation and movement. *J. Exp. Biol.* **215**, 2869-2880.

Domenici, P. and Blake, R. W. (1997). The kinematics and performance of fish fast-start swimming. *J. Exp. Biol.* **200**, 1165-1178.

Drucker, E. G. and Lauder, G. V. (2001a). Wake dynamics and fluid forces of turning maneuvers in sunfish. *J. Exp. Biol.* **204**, 431-442.

Drucker, E. G. and Lauder, G. V. (2001b). Locomotor function of the dorsal fin in teleost fishes: experimental analysis of wake forces in sunfish. *J. Exp. Biol.* **204**, 2943-2958.

Drucker, E. G. and Lauder, G. V. (2005). Locomotor function of the dorsal fin in rainbow trout: kinematic patterns and hydrodynamic forces. *J. Exp. Biol.* **208**, 4479-4494.

Epps, B. and Techet, A. (2007). Impulse generated during unsteady maneuvering of swimming fish. *Exp. Fluids* **43**, 691-700.

Geerlink, P. J. and Videler, J. J. (1986). The relation between structure and bending properties of teleost fin rays. *Neth. J. Zool.* **37**, 59-80.

Jayne, B. C., Lozada, G. F. and Lauder, G. V. (1996). Function of the dorsal fin in bluegill sunfish: Motor patterns during four distinct locomotor behaviors. *J. Morphol.* **228**, 307-326.

Kreyszig, E. (1991). *Differential Geometry*. New York, NY: Dover Publications.

Lauder, G. V. (2006). Locomotion. In *The Physiology of Fishes* (ed. D. H. Evans and J. B. Claiborne), pp. 3-46. Boca Raton, FL: CRC Press.

Lauder, G. V. and Drucker, E. G. (2004). Morphology and experimental hydrodynamics of fish fin control surfaces. *IEEE J. Oceanic Eng.* **29**, 556-571.

Lauder, G. V. and Madden, P. G. A. (2007). Fish locomotion: Kinematics and hydrodynamics of flexible foil-like fins. *Exp. Fluids* **43**, 641-653.

Lauder, G. V., Madden, P. G., Mittal, R., Dong, H. and Bozkurttas, M. (2006). Locomotion with flexible propulsors: I. Experimental analysis of pectoral fin swimming in sunfish. *Bioinspir. Biomim.* **1**, S25-S34.

Lauder, G. V., Madden, P. G. A., Tangorra, J. L., Anderson, E. and Baker, T. V. (2011). Bioinspiration from fish for smart material design and function. *Smart Mater. Struct.* **20**, 094014.

Mittal, R., Dong, H., Bozkurttas, M., Lauder, G. and Madden, P. (2006). Locomotion with flexible propulsors: II. Computational modeling of pectoral fin swimming in sunfish. *Bioinspir. Biomim.* **1**, S35-S41.

Osburn, R. C. (1906). The functions of the fins of fishes. *Science* **23**, 585-587.

Ramamurti, R., Sandberg, W. C., Löhner, R., Walker, J. A. and Westneat, M. W. (2002). Fluid dynamics of flapping aquatic flight in the bird wrasse: three-dimensional unsteady computations with fin deformation. *J. Exp. Biol.* **205**, 2997-3008.

Reinschmidt, C. and van den Bogert, T. (1997). KineMat: a MATLAB toolbox for three-dimensional kinematic analyses. Calgary, Canada: Human Performance Laboratory, The University of Calgary.

Rice, W. R. (1989). Analyzing tables of statistical tests. *Evolution* **43**, 223-225.

Sokal, R. R. and Rohlf, F. J. (1981). *Biometry*. New York: W. H. Freeman.

Standen, E. M. and Lauder, G. V. (2005). Dorsal and anal fin function in bluegill sunfish *Lepomis macrochirus*: three-dimensional kinematics during propulsion and maneuvering. *J. Exp. Biol.* **208**, 2753-2763.

Taft, N. K., Lauder, G. V. and Madden, P. G. A. (2008). Functional regionalization of the pectoral fin of the benthic longhorn sculpin during station holding and swimming. *J. Zool. (Lond.)* **276**, 159-167.

Tytell, E. D. and Lauder, G. V. (2008). Hydrodynamics of the escape response in bluegill sunfish, *Lepomis macrochirus*. *J. Exp. Biol.* **211**, 3359-3369.

Wakeling, J. M. (2001). Biomechanics of fast-start swimming in fish. *Comp. Biochem. Physiol.* **131A**, 31-40.

Walker, J. A. (1998). Estimating velocities and accelerations of animal locomotion: a simulation experiment comparing numerical differentiation algorithms. *J. Exp. Biol.* **201**, 981-995.

Walker, J. A. (2004). Kinematics and performance of maneuvering control surfaces in teleost fishes. *IEEE J. Oceanic Eng.* **29**, 572-584.

Walker, J. A. and Westneat, M. W. (2002). Performance limits of labriform propulsion and correlates with fin shape and motion. *J. Exp. Biol.* **205**, 177-187.

Zar, J. H. (1984). *Biostatistical Analysis*. Englewood Cliffs, NJ: Prentice Hall.